Analysis of satellite and model datasets for variability and trends in Arctic snow extent and depth, 1948–2006

Hotaek Park,[1*] Hironori Yabuki,[1] and Tetsuo Ohata[1]

* corresponding author

[1] Research Institute for Global Change, JAMSTEC, 2-15 Natushimacho, Yokosuka, 237-0061, Japan

Abstract

This study aims to investigate the spatiotemporal trends in snow depth (SD) and snow cover extent (SCE) for Arctic lands, except Greenland, during 1948–2006. The investigation not only delineates Arctic regions undergoing significant annual trends in both SD and SCE, but also provides a comprehensive understanding of their historical trends and patterns. For these objectives, a coupled hydrological and biogeochemical model (CHANGE), NOAA weekly SCE data, and *in situ* observation of SD were used. Most regions in the Arctic exhibited a significant negative trend in SD over the 59 years. The magnitude of the negative trend was stronger in North America than in Eurasia, where the decrease was mostly significant since the late 1980s coinciding well with the temperature rise. During the same period, the warming temperature caused a prominent decrease in deeper SDs (i.e., > 35 cm), so that their SCEs exhibited negative anomalies, with the greatest declines at > 55 cm of SD. By contrast, SCEs of SD ≤ 35 cm showed increasing anomalies during the recent two decades, in which the increase means the sequential result induced by the decrease in SCEs of deeper SDs, rather than the expansion of snow to snow-free region. These

changes resulted in a northward shift of the shallow SD line, which was greatly significant in North America. These results suggest that the changes of the Arctic SCE and SD will be more intensified under the future climate warming.

Keywords: snow depth, snow cover extent, Arctic lands, spatiotemporal variability, land surface model, satellite data

1. Introduction

Snow is a vital component of the Arctic regions because its large seasonal variations and distinctive physical properties greatly affect climate, hydrology, and ecology at regional and global scales. The influence of snow on the Arctic system is present through interactions with other components within the system. The manifestations are positive albedo feedback (Groisman et al., 1994; Déry and Brown, 2007) and other feedback related to moisture storage, latent heat, and soil insulation (Stieglitz et al., 2003). The snow-albedo feedback is linked to the radiative budget (Groisman et al., 1994) and influences temperature over a broad land surface, which in turn affects atmospheric circulation and climate. This interaction is invoked as a leading cause of amplified warming in Arctic regions, especially in polar and mountainous regions (Serreze and Francis, 2006).

Snow depth (SD) is a key variable to understand the evolution of the Arctic hydrological cycle. Arctic river discharge is mainly driven by the accumulated SD and depends on the timing of its melting, which may lead to extensive floods in spring (Yang et al., 2003). Climate change significantly influences the process of snow accumulation and ablation. Barnett et al. (2005) have projected that an acceleration of the hydrological cycle due to global warming in snow-dominated regions will cause earlier snowmelt and maximum SD timing that may lead to regional water shortages. The strong link between snow cover extent (SCE), SD, and river discharge has been investigated for Siberian watersheds (Yang et al., 2003) and northern Canada (Déry et al., 2005).

Recent research indicates a significant decrease in snow over North America during winter, in response to rising air temperatures (Dyer and Mote, 2006). By contrast, long-term *in situ* measurements for Eurasia exhibit increasing SD trends (Bulygina et al., 2009; Kitaev et al., 2005). The observations suggest that the Arctic regional snow depth response appears less consistent with the Arctic warming trend. However, few *in situ* snow depth datasets for the Arctic regions are available, providing limited information on spatiotemporal snow depth fields. Remote sensing techniques are used to complement the *in situ* data. For instance, satellite data have revealed that Arctic spring SCE has experienced a rapid decrease since the start of satellite observations, as has been well documented (Brown et al., 2010). SCE from remote sensing images provides information only about whether snow appears or not. Therefore, SCE but partially characterizes snow variability. Unfortunately, the fewest studies had dealt with the variability in the complete spatial coverage of the snow depth evaluation over the Arctic.

Although the Special Sensor Microwave/Imager (SSM/I) has provided radiometric measurements concerning snow depth changes over the Arctic land surfaces since 1989, the data record is perhaps still too short for studies regarding interannual to multidecadal changes in SD. The weekly SCE charts of NOAA were derived from manual interpretation of visible satellite imagery. The presence/absence of snow over the Northern Hemisphere was determined based on a 50% snow cover threshold in each grid cell. SSM/I-derived SCE includes the large uncertainties/errors, especially in heavily vegetated areas (e.g., the boreal forest). Brasnett (1999) found that a lower 30% threshold was required to emulate the snow-covered area in the NOAA analysis so there is built-in conservatism in the product particularly in mountain regions. Modeling represents a convenient and complementary approach for assessing spatiotemporal patterns of SD and SCE changes. Hirabayashi et al. (2005) pointed that trends of snow covered area over North America and Eurasia after the 1970s seen in satellite-based observation do not exceed ranges within past variation obtained by an off-line land surface model simulation between 1901-2000. However, modeling results also entail problems, which are sensitive to the forcing data and parameters. Therefore, a combined use of field observations, satellite data, and modeling results likely expands the opportunity to explore SD and SCE trends in the Arctic on continental scales. The combination also makes it possible to investigate the degree of consistency between the satellite data and the modeling results in terms of the spatiotemporal variability of SD and SCE.

The main objective of this study is to investigate the spatiotemporal trends and variability in SD and SCE for the Arctic terrestrial regions, excluding Greenland, over the past 59 years (1948–2006) by using a combination of land surface model simulation, satellite-based observation, and field observation. The investigation not only delineates Arctic terrestrial regions undergoing significant annual trends in both SD and SCE, but also provides a comprehensive understanding of their historical trends and patterns. Snow variations in response to climatic forcing likely provide an insight to project the variability of SD and SCE in the future under climate change.

2. Model description

The coupled hydrological and biogeochemical model (CHANGE) used in this study is a physically based land surface model designed to integrate the interactions and feedback effects in a soil-vegetation-atmosphere system in the Arctic terrestrial regions. CHANGE includes the following processes: spatiotemporally varying exchanges of energy, water, and CO_2 at the soil-vegetation-atmosphere interfaces; snow accumulation and melting; soil freezing and thawing; effects of ice on soil water flux; effects of soil organic matter on water and heat fluxes; and vegetation dynamics, including the carbon and nitrogen budgets of the ecosystem. To integrate the interactions within a complex soil-vegetation-atmosphere system, CHANGE is designed using a modular structure and consists of four modules for land surface, vegetation phenology, carbon-nitrogen balance, and vegetation dynamics. The full description of CHANGE is given by Park et al. (2011), but snow processes are briefly described here.

The land surface module essentially solves the energy and mass balances for the canopy, snow, and soil over a gridded domain. Therefore, snow processes are closely connected not only to radiation, energy, and water budgets of the canopy layer and soil layers, but also to vegetation dynamics. The main snow processes represented in the model are shown schematically in Fig. 1. Snowpacks are naturally layered media, so CHANGE represents the snowpack as two layers, with a thin surface layer and a thick deeper layer (Anderson, 1976; Wigmosta and Lettenmaier, 1994). The thin surface layer is used to solve the surface energy balance, while the pack layer is used to simulate deeper snowpacks. The surface energy balance components are used to simulate melting, refreezing, and changes in the snowpack heat content. The mass balance components represent snow accumulation or ablation, changes in snow water equivalent, and snowpack water yield. The snowpack energy balance is given by

$$c_{ice}\rho_w \frac{dw_{sp}T_{sp}}{dt} = Q_n + Q_s + Q_l + Q_p + Q_m + Q_g \qquad (1)$$

where c_{ice} is the specific heat of ice, ρ_w is the water density, w_{sp} is the snowpack water storage, Q_n is the net radiation, Q_s is the sensible heat transfer by turbulent convection, Q_p is the heat advected into the snowpack by rainfall, and Q_g is the heat transferred by conduction from the snow-ground interface. Further, Q_l is the energy lost to evaporation and sublimation or gained through latent heat release during condensation, while Q_m is the internal latent heat lost to melting or gained through liquid water refreezing. The left-hand term in (1) denotes the change in snowpack heat content. For components on the right-hand side of (1) and the related equations refer to Park et al. (2011). Equation (1) is solved at time steps through a forward finite difference scheme in which snow surface temperature (T_{sp}) is iteratively calculated.

The net radiation at the snow surface is calculated from the budget of net shortwave and longwave radiations. Because the canopy and soil usually have different spectral properties for individual spectral bands, the shortwave radiation is decomposed into direct beam and diffuse radiation. Albedo is calculated for the canopy and the ground surface by using the two-stream approximation (Meador and Weaver, 1980), wherein the overall direct beam and diffuse ground albedos are weighted using combinations of soil and snow albedos. The net radiation is divided into the right-hand terms of (1). The heat flux through the snowpack, Q_g, was added to couple the snow and frozen soil. Temperatures within the snowpack are assumed to follow a linear profile. However, taking into account that the soil surface temperature is allowed to change, the balance of fluxes at the surface is given by

$$k_s \frac{dT_{sp}}{dSD} = G = -k \frac{dT}{dz}\bigg|_{z=0} \tag{2}$$

where k_s is the thermal conductivity of snow (Jordan, 1991), dT_{sp} is the change in temperature from the snow surface to the ground surface, k is the thermal conductivity of the soil, and dSD is the change in the snowpack depth.

The total energy available from refreezing liquid water or for melting snowpack over a given time step depends on the net energy exchange at the snow surface, derived from (1) as

$$Q_m = \left(Q_n + Q_s + Q_l + Q_p + Q_g\right)\Delta t \, . \tag{3}$$

If Q_m is negative, then energy is lost by the snowpack, and liquid water (if present) is refrozen ($w_{sp,liq}$). If Q_m is sufficiently negative to refreeze all liquid water, the snowpack may cool. If Q_m is positive, the excess energy produces snowmelt ($w_{sp,ice}$).

The mass balance of the snowpack takes into account two phases (liquid and ice) whose mass balances are given by

$$\Delta w_{sp,liq} = P_r + \frac{Q_l}{\rho_w \lambda_v} - \frac{Q_m}{\rho_w \lambda_f} \tag{4}$$

$$\Delta w_{sp,ice} = P_s + \frac{Q_l}{\rho_w \lambda_s} - \frac{Q_m}{\rho_w \lambda_f} \tag{5}$$

where λ_s and λ_v are the latent heats of sublimation and vaporization, respectively, P_r is the rainfall depth, and P_s is the water equivalent of the snowfall. Precipitation is partitioned into snowfall and rainfall based on a temperature threshold given by Wigmosta and Lettenmaier (1994). When $w_{sp,ice}$ exceeds the maximum thickness of the surface layer, the excess is distributed to the deeper pack layer. Similarly, the portion of $w_{sp,liq}$ that exceeds the liquid water holding capacity of the surface layer is drained to the pack layer. Liquid water remaining in the pack layer and exceeding the maximum holding capacity is immediately routed to the soil as snowpack outflow. However, as the temperature of the pack layer is below freezing, liquid water in the pack is refrozen. During the snowmelt, either the atmosphere exchanges water with the liquid phase or the atmosphere exchanges water vapor with the ice phase in the absence of liquid water.

As snow accumulates on the ground, the snowpack compacts and its density increases over time. In addition to this change in density, gravitational settling caused by newly fallen snow also contributes to the densification of the snowpack with age. Following an approach similar to that of Anderson (1976), the compaction is calculated as the sum of the two fractional compaction rates due to metamorphism and overburden.

The metamorphism is important for newer snow, but after the initial settling stage the densification rate is controlled by the snow overburden through load pressure. Within a layered snowpack, the load pressure would be different for pack layers corresponding to different compaction rates, which represents that internal compaction is effective as load pressure.

Snow depth is not directly computed in CHANGE but is needed in the calculation of the heat flux through the snowpack. Hence, the depth of the snowpack is simulated using a snow water equivalent (*SWE*), with the density of the snowpack influenced by compaction and metamorphism. That is,

$$\Delta SD = \frac{P_s \cdot SD}{SWE}\left[\frac{SD}{10}\right]^{0.35} \tag{6}$$

where ΔSD is the change in SD. The density of new snow is taken as 50 kg m^{-3}, unless the air temperature is above 0°C, in which case the snow density increases as a function of temperature (Anderson, 1976).

When snow falls, it is primarily intercepted by the canopy, where sublimation, mass release, and snowmelt occur. The processes of snow interception are included in CHANGE, based on the algorithm of Storck et al. (2002). The snowmelt from the canopy is calculated from the energy balance between the estimated surface temperature and the observed air temperature. The surface temperature of the canopy snowpack is solved iteratively with a modified energy balance, in a similar manner as for the ground snowpack (Eq. (1)). Snowmelt in excess of the liquid water holding capacity of the snow results in meltwater drip. Mass release from the canopy snowpack occurs if sufficient snow is available and is related linearly to the production of meltwater drip (Storck et al., 2002).

Separate aerodynamic resistances are calculated for the canopy, ground surface, and snow surface. When a canopy exists, the vertical wind velocity profile is modeled using three layers (Campbell, 1977). A logarithmic wind speed profile is used above the canopy. Wind speed is assumed to decrease exponentially through the canopy, merging into a new logarithmic profile near the ground or snow surface. When snowpack appears, the calculation of turbulent energy exchange is complicated by the stability of the atmospheric boundary layer. If the snowpack is colder than the atmosphere (stable condition), parcels of cooler air near the snow surface transported upward by turbulent eddies tend to sink back toward the surface, thus suppressing turbulent exchange. In unstable (lapse) conditions, vertical motion is enhanced by buoyancy. In the presence of a snowpack, therefore, aerodynamic resistance is corrected for the atmospheric stability according to the bulk Richardson's number that is a dimensionless ratio relating the buoyant and mechanical forces (i.e. turbulent eddies) acting on a parcel of air (Anderson, 1976).

In wind-swept regions, snow transport by blowing causes snow cover redistribution and water loss by sublimation fluxes. The transport and sublimation result in losses of from 30% to 75% of the annual snowfall in prairie, steppe, and tundra regions (Pomeroy et al., 1997). Considering the importance of blowing snow, CHANGE is coupled with an algorithm for blowing snow (Pomeroy and Li, 2000), which calculates transport and sublimation fluxes using standard meteorological and land-cover data. Scaled-up blowing snow transport and sublimation fluxes are used to calculate open environment snow accumulation by accounting for variability over open snowfields, increases in transport and sublimation with fetch, and the effect of exposed vegetation on partitioning the shear stress available to drive transport. The scaled blowing snow fluxes are used to calculate the snow mass balance and to simulate seasonal snow accumulation. Because the spatial resolution of the model is relatively coarse (0.5° × 0.5°), snow transport between grids is not considered in the simulation. Instead, all of the snow transport caused by the blowing is assumed to be sublimation lost from the grid cell.

3. Model application and dataset

The CHANGE model was applied to the Arctic lands for the period of 1948–2006 with a spatial resolution of 0.5° × 0.5°. The Arctic is defined as the land area north of 45°N and 0–360°E. Inputs to the model include information about vegetation type, soil texture, and atmospheric climate. The vegetation type in each grid cell was based on the vegetation map given by Ramankutty and Foley (1999), which recognizes 15 types. Ice cover was not considered in the simulation and thus Greenland was not included. CHANGE also requires soil texture information in terms of the fractions of sand, silt, and clay. We derived the data from the IGBP SoilData System (Global Soil Data Task, 2000). The texture fractions are combined with soil organic matter data to estimate the thermal conductivity, heat capacity, and hydraulic conductivity of the soil. The gridded climate dataset used in this study had a global spatial resolution of 0.5^{o} and a daily resolution from 1948 to 2006 (Hirabayashi et al., 2008; H08). This includes air temperature (mean, maximum, and minimum), precipitation, specific humidity, solar radiation, and wind speed. The gridded climate forcing was interpolated with station measurements of monthly temperature and precipitation (Hirabayashi et al., 2005). The monthly temperature was sourced from Climatic Research Unit (CRU) Ts 2.1 extended with both Glogbal Historical Climatology Network (GHCN) and NOAA CPC Climate Anomaly Monitoring System (CAMS) monthly gridded data. The monthly precipitation includes NOAA CPC station data and Global Precipitation Climatology Centre (GPCC) ver. 5. Daily shortwave radiation product of the Surface radiation Budget (SRB) was used to derive daily grid shortwave radiation forcing. Hirabayashi et al. (2005) well described the disaggregation of monthly climatic variables into a daily time series using a stochastic weather generator. The 6-hourly surface wind data for the period of 1958-2001 from European Centre for Medium-Range Weather Forecasts (ECMWF, ERA-40) were averaged to the daily for each grid cell, then wind data of 2.5°× 2.5° were interpolated to 0.5° × 0.5°.

The averaged daily grid wind was in turn averaged for the annual 365 (or 366) days based on the period 1958-2001. The averaged annual wind was used for the remaining simulation years except 1958-2001. We downscaled this daily climate data to hourly data in order to accommodate the time step required by CHANGE. Park et al. (2011) have described well the hourly interpolation process for each variable. Park et al. (2011) also found that a constant diurnal relative humidity can significantly overestimate latent heat flux. Thus, an algorithm developed by Castellví et al. (1996) was used to interpolate the diurnal relative humidity.

The thermal and hydrological regimes of the ground and the vegetation components must be initialized for each grid cell. Since there are no detailed measurements for model initialization, the initial conditions were determined by spin-up runs. The initial assumptions included no snow, no soil carbon, and very little vegetation carbon. The initial soil moisture was set to 0.3 in all soil layers. The initial soil temperature profile was exponentially interpolated using the starting date air temperature at the surface and the mean annual air temperature at the bottom. The spin-up runs were repeated until the total ecosystem carbon flux reached a steady state after running for approximately 420 years using the forcing data of the initial 20 years and a pre-industrial CO_2 concentration of 300 ppm.

We also used the NOAA weekly snow cover data to generate SCE time series over the Arctic regions for the period 1966–2006. The NOAA weekly product derived from manual interpretation of visible satellite imagery has been well described by Robinson et al. (1993). On the basis of these weekly records, we examined the monthly SCE variability within long-term time series. The long-term monthly SCE data were compared with the modeled SCE and were used to examine the relationship between SCE and SD.

The performance of SD calculated by CHANGE was thoroughly investigated for 9 years of a Siberian larch forest (Park et al., 2011). However, the Arctic regions to which CHANGE was applied in this study have very different climates and land surface conditions. Before analyzing the trends and variability in SD and SCE, we first compared the simulated results with observations under various conditions. The dataset of the Global Surface Summary of the Day (GSOD), archived at the National Climatic Data Center (NCDC, http://www.ncdc.noaa.gov/), includes SD data observed at meteorological stations worldwide. Thus, 518 stations that located at >45°N and recorded 10 or more years of SD data were selected for the comparison of the model results. The SD at each station was averaged over January to March (JFM) for each year of the period available.

4. Results and Discussion

4.1 Climatic conditions

Winter (October to March) time series of air temperature and precipitation over the Arctic lands are shown in Fig. 2. The Arctic temperature exhibited an increasing trend, reaching 1.8°C in 2002 and 1.62°C in 2006, historically the warmest years. The years next to those years were associated with the minimum Arctic sea ice cover. Over the last several decades, Arctic warming became stronger, especially after the late 1970s (Fig. 2). Over the 59-year period 1948–2006, the winter temperature increased 0.31°C per decade, but the increase after 1979 was 0.42°C per decade. Based on *in situ* observations over the Northern Polar Area (NPA), Bekryaev et al. (2010) found that positive trends in NPA winter temperatures over longer time series were very strong, as much as 1.73°C per century for 1875–2008. The warming since the late 1980s was stronger in the autumn and winter than in the summer (Fig. 3). During the same period, the temperature increase in the spring was also strong (Fig. 3).

Winter time series of precipitation exhibit the larger interannual variability compared to temperature. The strongest negative anomalies in precipitation were observed during 1948–1954, but thereafter the anomalies became positive, reaching a maximum value in 1967. From 1970, the precipitation had a cycle of increasing and decreasing that repeated with a timescale of 5–10 years. Among the precipitation cycles, those after 1995 indicated the greatest interannual variability. Precipitation showed a weak increasing trend during the period 1948–2006, although this was not statistically significant. Precipitation during 1948–1970 showed a significant increasing trend at the $\geq$ 95% confidence level, while precipitation after 1990 tended to decrease.

4.2 Comparison between simulations and observations of snow depth

The GSOD data included the daily SD at each site, which was averaged for JFM of individual years. The simulated SD was also averaged for the four grid pixels around the GSOD sites by weighting for distance. The treated annual means were compared between observations and simulations, and then the correlation coefficients were derived from the comparisons at individual sites (Fig. 4). The correlation coefficients that were significant at the ≥ 95% confidence level are colored in Fig. 4(a). Sites with significant correlation coefficients are mainly located inland, where the land cover was mainly classified as forest. At northern sites, where the density of SD observation stations was considerably lower, the correlations tended to be lower than at southern sites.

The annual JFM mean SD of individual GSOD sites was in turn averaged over the period of availability. Correspondingly, the simulated values were averaged over the period consistent with the observations. Fig. 4(b) compares the averaged SD results of the observations and simulations. Although the comparison reveals a large scatter, CHANGE estimates the SD moderately well. The deviation might be explained by the difference in scale between the simulations and the observations. For complex terrains, point observations extrapolated to obtain large-area averages tend to be poorly representative of true area means (Nelson et al., 1997). Scale issues are encountered with differences in elevation, which fundamentally influence precipitation and temperature. The difference in land surface conditions is another reason for discrepancies between the simulations and the observations. Many GSOD sites measured SD in the open, while the grid pixels around the GSOD sites in the simulation were associated with forest. Therefore, the comparison should be viewed as a general assessment of model performance rather than a precise test.

4.3 Snow depth trends

The snow depth for JFM in individual grid pixels was averaged over the period 1948–2006. Fig. 5(a) shows the spatial distribution of the averaged SD, displaying large regional heterogeneity. A linear regression analysis was performed on each grid for the annual SD averages during 1948–2006. The results of the trend analysis (Fig. 5b) show a large regional heterogeneity. During the study period, the snow depth generally exhibited a decreasing trend, except for locally increasing regions in Western Siberia (e.g., especially the Yenisey and Ob watersheds) and in the northwestern area of Hudson Bay (Fig. 5b). Bulygina et al. (2009) reported that the maximum SD at 820 *in situ* stations across Russia increased from 0.2 cm yr^{-1} to 0.6 or 0.8 cm yr^{-1} between 1966 and 2007 (with maximum rates in Western Siberia). Based on *in situ* observations, Kitaev et al. (2005) found a positive SD trend (0.09 cm yr^{-1}) across Eurasia (for latitudes above 40°N) in February during 1936–2000. The increasing trend (< 0.5 cm yr^{-1}) of the simulated SD in Siberian regions falls within the ranges derived from the observations. The decreasing trend of SD in the North American regions was stronger than for Eurasian regions. Dyer and Mote (2006) found locally significant decreases (> 0.25 cm yr^{-1}) in the SD of northwestern Canada during 1960–2000. This decreasing SD over larger areas implies a response to rising air temperatures.

To integrally outline the spatiotemporal variability of SD during 1948–2006, we derived SD anomalies for 10-year intervals on a pixel-by-pixel basis (Fig. 6). Although some regions experienced below average increases, the Arctic terrestrial regions generally had positive SD anomalies until 1980. In particular, both Western Siberia and northwest regions of Hudson Bay exhibited the increasing trend during 1948–2006 (Fig. 5b). The Arctic coastal regions exhibited negative anomalies for 1951–1960, but these anomalies recovered to become positive for 1961–1970. Notably, the Arctic terrestrial regions were extensively covered by deeper snow during the period 1951–1980 when the Arctic experienced negative temperature anomalies and much precipitation (Fig. 2).

Snow depth has explicitly changed since 1980, when the SD predominantly shifted to negative anomalies, though some regions maintained weak positive anomalies until 1990. Thereafter, the negative SD anomalies of the Arctic regions became greater in both magnitude and extent. These negative anomalies were stronger in North America than in Eurasia. Satellite data reveal the SD decreasing over North America since 1990 while increasing over Eurasia (Biancamaria et al., 2011). *In situ* observations have also addressed the decrease in SD over North America in recent years (Dyer and Mote, 2006). The decrease in SD over North America may be the result of a combination of storm track and surface energy balance variability (Dyer and Mote, 2006). Isard et al. (2000) suggested that a positive phase of the Pacific North American (PNA) teleconnection during the winter (December–February) was correlated with the decrease in cyclone frequency in North America and therefore with the decrease in SD. During the winter, a large area of central Canada is strongly influenced by an influx of

Pacific moisture associated with a trough centered over the Gulf of Alaska, resulting in strong southwesterly geostrophic flow into the southern Mackenzie River basin (Serreze et al., 2003). It has also been shown that the variability of SD is sensitive to radiative balance (Groisman et al., 1994), surface energy fluxes (Dyer and Mote, 2002), and air temperature variations (Brown and Goodison, 1996). The winter air temperature in North America exhibited an increasing trend over 15 recent years (Bekryaev et al., 2010), which led to a decrease in SD. Dyer and Mote (2007) found that the increase in the frequency of snow ablation events is a cause for the decrease in SD over North America.

Regions that display anomalies opposite to those of their neighbors exist in the Ob, Yenisey, and Lena watersheds. Interestingly, these regions appear in most of the maps in Fig. 6, although the strength of the anomalies is different. The pattern of opposite anomalies in these regions has been significant since 1991. Serreze et al. (2003) outlined the characteristics of seasonal moisture circulations over these regions. According to the analysis of Serreze et al. (2003), variability in winter effective moisture over the Ob is closely allied with the strength and location of the Urals trough, but winter precipitation variations in the Lena and Yenisey basins are more closely associated with variability in the strength of the zonal flow. Moreover, the Eurasian watersheds (Ob, Yenisey, and Lena) have SD anomalies nearly opposite to those of the Mackenzie basin. Winter precipitation in the Mackenzie basin is lee-side cyclogenesis associated with a stronger than average zonal flow and a persistent influx of Pacific moisture (Serreze et al., 2003). Therefore, SD over North America and Eurasia is significantly correlated to the PNA and the Arctic Oscillation (AO), respectively (Biancamaria et al., 2011).

Arctic warming resulted in later snow accumulation in the fall and earlier snowmelt in the spring (Fig. 7). Earlier snow accumulation lasted until the 1980s. After 1989, however, the overall pattern of snow accumulation changed to a later timing due to the warming (Fig. 3). The late snow accumulation was even more significant after 2000, with a maximum of 8 days over the Arctic terrestrial regions (53°–70°N). Arctic warming in autumn, as identified in Fig. 3, has been addressed by many studies (Bekryaev et al., 2010; Screen and Simmonds, 2010). Screen and Simmonds (2010) determined that the warming in autumn is closely related to the diminishing Arctic sea ice, and the influence extends to 45°N. Satellite-based analysis for 1972–2000 revealed no evidence of any systematic trend in the first snow date over the Arctic (Dye, 2002). However, Russian *in situ* observations indicated a trend for earlier first snow during 1937–1994 (Ye, 2001). Ye (2001) explained that the earlier snowfall in autumn might be related to the decreasing trends in solar radiation and northern land surface air temperatures in autumn during 1945–1986. When compared to our study, the different trends in the autumn SD may be associated with the difference in the individual study periods.

The earlier snowmelt in the spring was mostly significant after 1990 (Fig. 7b), when the spring snow disappearance was earlier by a maximum of 8 days, which reveals the strong sensitivity to warming (Fig. 3). Evidently, both *in situ* observations (Dyer and Mote, 2006; Groisman et al., 2006) and satellite observations (Dye, 2002; Brown et al., 2010) captured the earlier snowmelt over the Arctic regions. Dye (2002) found that the spring snow disappearance over the Arctic was earlier by 3–5 days per decade for 1972–2000. Over central Canada, *in situ* observation-based gridded data have indicated that the regional decreases in spring snow depth are likely a result of more rapid melting of shallower winter snowpack (Dyer and Mote, 2006).

Effects related to the later first snowfall and earlier snowmelt have been found in various processes of the Arctic terrestrial ecosystems. The later snow accumulation likely decreases thermal insulation of soil by snow (Iijima et al., 2010), while the earlier snowmelt can potentially cause earlier soil thawing (McDonald et al., 2004). There was a negative correlation between the spring snowmelt dates and the normalized difference vegetation index (NDVI) of the growing season over central Siberia (Grippa et al., 2005), because the shorter growing season due to later snowmelt reduced the subsequent CO_2 capture in summer (Llody and Fastie, 2002). Both the later snowfall and the earlier snowmelt consequently lengthened the growing season, which may positively correlate to vegetation productivity. Changes in snowmelt pattern can also affect the associated peak floods and therefore cause a shift in hydrologic regime. In fact, a late snowmelt in Siberian watersheds has been associated with a high flood peak (Yang et al., 2003).

4.4 Snow cover extent trends

NOAA provides weekly visible satellite observation data on Northern Hemisphere snow cover since 1966. Fig. 8(a) shows the monthly SCE time series over the Arctic during 1967–2006 for both the NOAA dataset and the model result. The comparison between NOAA data and the simulated results shows good agreement for SCE (Fig. 8a). The monthly SD time series (Fig. 8b) are computed from the model results as the area-weighted average SD over the Arctic. Substantial differences are observed in the seasonal and interannual variability of the two snow variables. Monthly mean SCE increases in the early snow season and reaches a maximum in January and February, but this exhibits almost no interannual variability since the entire region is essentially snow covered. The largest interannual variability of monthly SCE occurs during the autumn snow accumulation and the spring snowmelt. Likewise, the SD over the Arctic is subject to interannual variability. However, the timing and magnitude of SD variability is not necessarily consistent with SCE, because SD shows a steadily increasing variation with accumulation, peaking in February and March. Relatively large interannual variability of SD is observed during the peaks and the spring snowmelt season.

The different behaviors of these two snow parameters chiefly indicate that snow anomalies initially occur during the autumn accumulation and persist throughout the snow season. During the autumn or spring, snow is of limited spatial extent and is generally shallow, thus snowfall events and ablation processes affect both SCE and SD. During the mid-winter season, the Arctic is covered by relatively deep snowpack, so abrupt changes in SCE are rare. Instead, snowfall events and ablation processes can significantly alter SD in mid-winter. These results suggest that SCE during autumn and spring is closely associated with SD (Ge and Gong, 2008). Satellite data have indicated that mean SCE over the northern hemisphere was considerably less extensive after the mid-1980s (Robinson et al., 1993; Groisman et al., 1994). The greatest negative anomalies of SCE occurred in the spring and early summer, due to the increased air temperature (Robinson et al., 1993; Brown et al., 2010). Analysis of the NOAA weekly dataset reveals clear evidence of stronger reductions in spring snow cover in northern coastal regions (Brown et al., 2010), which likely coincides with enhanced local warming related to thinning sea ice (Lindsay et al., 2009) and earlier sea ice retreat (Howell et al., 2009). Similarly, the earlier snow disappearance over Arctic lands in spring has been identified for regions at 60° N and 70°N (Foster et al., 2008).

The variability of the monthly mean SD and SCE suggests that SD during the winter does vary independently of the snow extent, while the interannual variability of SD is likely associated with various parameters. To access the interannual patterns of SD over the Arctic, a hybrid analysis of SD and SCE was performed with the simulated results (Fig. 9). Snow depth was classified into various levels, and SCE was defined as the areal extent of the snow cover at the given SD level. The SCE was averaged for individual SD levels during both the study period of 1948–2006 and the defined periods at 10-year intervals. The SCE change rate means a ratio of the latter SCE average to the former. This analysis can provide information on the historical trend of SCE. Results of the SCE analysis are shown in Fig. 9, which exhibits the interannual variability of SCE for individual SD levels. The degree of the variability was relatively large at lower (≤ 5 cm) and higher (≥ 66 cm) SD levels. At the level of ≤ 5 cm, SCE became increasing after 1971. For instance, SCE during 2001–2006 increased 62.2% compared to the average. In contrast, SCE at the level of ≥ 66 cm transformed from increasing to decreasing over the length of the time series, showing the maximum decrease during

2001–2006.

The SCE at most SD levels of ≥ 36 cm exhibited negative anomalies after 1991 when temperature entered into the warming mode (Fig. 2a). The contrasting patterns are found at levels ≤ 35 cm (Fig. 9). Therefore, we defined the SD of 36–45 cm as a threshold level for SCE change involved in the climate change. Dyer and Mote (2006) found that in North America during 1960–2000 the most negative anomalies in SCE occurred at the SD level of 40–50 cm with a second peak at 2–10 cm. These results of Dyer and Mote (2006) are very similar to ours. The increasing SCE of shallower snowpack (≤ 35 cm) during the recent two decades is likely a result of the decrease in deeper snowpack. To better illustrate the changes in SCE, the areal extent of snow cover for two SD levels (≤ 5 cm and ≥ 36 cm) was compared between two periods with relatively deep snowpack (1961–1970) and relatively shallow snowpack (2001–2006). The comparisons are displayed in Fig. 10, where the brown color represents SCE coexisted during the two periods. Blue indicates the extended SCE during 1961–1970, compared to 2001–2006. Therefore, blue and brown exhibit the total SCE during 1961–1970, and the total of green and brown represents during 2001–2006. SCE at

≤ 5 cm (Fig. 10a) was shifted considerably northward during the period 2001–2006 as compared to 1961–1970 when SD of ≤ 5 cm hardly appeared. The northward movement of the snowline can explain the recent increase in SCE of shallower SD. This implies the retreat of SCE at the thicker SD levels rather than expansion of SCE into snow-free regions. In the case of SD ≥ 36 cm (Fig. 10b), SCE during the period 2001–2006 declined considerably as compared to 1961–1970, most significantly in North America. These comparisons suggest that the increases in SCE with shallower snowpack during recent decades are the sequential result induced by declines in deeper snowpack.

The significant negative anomalies in deeper snowpack have also been observed from *in situ* observations in North America (Brown 2000; Dyer and Mote, 2006) and correlated to both late snow occurrence and less precipitation. Moreover, the winter temperature increase may advance the speed of snowmelt. However, despite the negative SD anomalies identified for Eurasia during 2001–2006 (Fig. 6), no large decrease in SCE of ≥ 36 cm over Eurasia was discerned (Fig. 10b), although it decreased in some regions. The SD of Eurasian regions marked on Fig. 10(b) was, on average, deeper than 35 cm (Fig. 5a). Therefore, the negative SD anomalies during the period (Fig. 6) are not as large an influence on SCE. However, the spring SCE is not necessarily consistent with the winter SD trend. During the snowmelt season, the deeper snowpack requires more energy to melt the snowpack, and this might compensate for the greater availability of energy (sensible heat) that would otherwise act to melt the snow sooner (Foster et al., 2008). Satellite data indicate the melting season over Eurasia has been advancing since the start of observations (Foster et al., 2008; Brown et al., 2010).

4.5 Variability of SD and SCE under climate change

Snow cover is anticipated to decrease in response to global warming, as snow accumulation and melting are greatly sensitive to a temperature threshold of 0°C. The temperature rise has resulted in both later snow accumulation in fall and earlier melting in spring. Consequently, the snow cover duration is shorter. These phenomena have mostly been evident since the mid-1980s (Fig. 7) when the Arctic amplification became significant (Serreze and Francis, 2006). When the Arctic warming is projected, increases in precipitation are predicted, especially at high latitudes and high elevations.

The increase in precipitation is sufficient to offset reductions in snow cover duration (Groisman et al., 1994). However, the resultant mild winters of global warming might advance the initiation of snowmelt, as identified in North America (Dyer and Mote, 2006). These changes would have regional sensitivities, since SCE and SD represented a highly localized variability during the past 59 years. This suggests that a combination of the projected higher winter precipitation and earlier spring snowmelt might increase the frequencies and severities of spring floods under the future climate change.

Both the areal extent and the duration of snow cover are more closely linked to albedo feedbacks, which are stronger during the spring (Groisman et al, 1994; Déry and Brown, 2007). Earlier snowmelt in the spring enhances available energy, increasing surface temperature. This can affect the near surface permafrost. Furthermore, the later snow accumulation combined with the earlier snowmelt allows a longer active layer melt season and thinner permafrost. In contrast, the shorter winter reduces thermal insulation of soil by snow, increasing soil freezing. However, the temperature increase during the spring and summer might offset the soil freezing, since higher soil moisture induced by the projected deeper snowpack may increase soil thermal conductivity.

The climatic impact of the Eurasian snow cover is not limited to regional scale: interannual land surface snow anomalies in this region can influence the interannual variability of the winter mode of the AO (Saito and Cohen, 2003; Saito et al., 2004; Gong et al., 2004). However, the AO in JFM changed to a strongly positive mode in the late 1980s, which is consistent with the earlier spring snowmelt tendencies (Foster et al., 2008). This suggests that the resultant earlier snowmelt associated with the global warming would have a compensatory positive impact on the AO.

5. Conclusion

This study examined spatiotemporal trends in SD and SCE over the Arctic regions during a 59-year period and quantified the magnitude of the interannual variability with a combination of satellite observations and modeling results. Most regions in the Arctic exhibited a significant negative trend in SD for the 59 years, significantly stronger in North America than in Eurasia. The patterns of the snow parameters in the snow season evidently changed after the late 1980s in good agreement with the warming patterns. During the same period, SCEs of deeper snowpack exhibited negative anomalies. The greatest decrease was identified at ≥ 55 cm of SD, while contrasting increases in SCE were observed at ≤ 35 cm. The increase in SCE of shallower SD in the two recent decades is likely a sequence induced by the decrease in SCE of deeper SD. This reflects the northward shift of a shallower SD line, which was more significant in North America than in Eurasia.

The results of this study demonstrate that the warming has decreased SD and SCE in the winter. Their decreases likely contribute to the rapid snow melt in spring. The decreases in SCE in the spring have consequences in the radiative balance. Due to variations in net radiation induced by albedo feedback, the surface temperature increases and therefore soil thawing is enhanced. However, this study provides evidence that localized changes in SCE and SD are occurring, which affects regional hydrologic systems due to a change in the availability and release of snowmelt runoff. The localized Arctic SD variability suggests an uncertainty in how future Arctic warming will affect snow processes. The dependence of precipitation, including snow, on atmospheric dynamics also enhances the uncertainty of the magnitude or amplitude of future snow changes. However, it should be noted that earlier snowmelt of shortened duration when combined with thicker SD might increase the frequencies and severities of spring floods in the future.

References

Anderson E. 1976. A point energy and mass balance model of a snow cover. *Tech. Rep. 19*. National Oceanic and Atmospheric Administration, Washington, DC.

Barnett T., Adam J. & Lettenmaier D. 2005. Potential impacts of a warming climate on water availability in snow-dominated regions. *Nature*. *438*, 303-309.

Bekryaev R., Polyakov I. & Alexeev V. 2010. Role of polar amplification in long-term surface air temperature variations and modern Arctic warming. *J. Clim*. *23*, 3888-3906, doi:10.1175/2010JCLI3297.1.

Biancamaria S., Cazenave A., Mognard N., Llovel W. & Frappart F. 2011. Satellite-based high latitude snow volume trend, variability and contribution to sea level over 1989/2006. *Global Planet. Change*. *75*, 99-107, doi:10.1016/j.gloplacha.2010.10.011.

Brasnett B. 1999. A global analysis of snow depth for numerical weather prediction. *J. Appl. Meteorol.*, *38*, 726-740.

Brown R. 2000. Northern Hemisphere snow cover variability and change, 1915-97. *J. Clim*. *13*, 2339-2355.

Brown R. & Goodison B. 1996. Interannual variability in reconstructed Canadian snow cover, 1915 – 1992. *J. Clim. 9*, 1299-1318.

Brown R., Derksen C. & Wang L. 2010. A multi-data set analysis of variability and change in Arctic spring snow cover extent, 1967-2008. *J. Geophys. Res.* 115, D16111, doi:10.1029/2010JD013975.

Bulygina O., Razuvaev V. & Korshunova N. 2009. Change in snow cover over northern Eurasia in the last decades. *Environ. Res. Lett.* 4, 045026, doi:10.1088/17489326/14/4/045026.

Campbell G. 1977. *An Introduction to Environmental Biophysics*, 159 pp., Springer-Verlag, New York.

Castellví F., Perez P., Villar J. & Resell J. 1996. Analysis of methods for estimating vapor pressure deficits and relative humidity. *Agri. For. Meteorol. 82*, 29-45.

Dery S., Sheffield J. & Wood E. 2005. Connectivity between Eurasian snow cover extent and Canadian snow water equivalent and river discharge. *J. Geophys. Res.* 110, D23106, doi:10.1020/2005JD006173.

Déry S. & Brown R. 2007. Recent Northern Hemisphere snow cover extent trends and implication for the snow-albedo feedback. *Geophys. Res. Lett. 34*, L22504, doi:10.1029/2007GL031474.

Dye, D. 2002. Variability and trends in the annual snow-cover cycle in Northern Hemisphere land areas, 1972-2000. *Hydrol. Proc. 16*, 3065-3077, doi:10.1002/hyp.1089.

Dyer J. & Mote T. 2002. Role of energy budget components on snow ablation from a mid-latitude prairie snowpack. *Polar Geogr. 26*, 87-115.

Dyer J. & Mote T. 2006. Spatial variability and trends in observed snow depth over North America. *Geophys. Res. Lett. 33*, L16503, doi:10.1029/2006GL027258.

Dyer J. & Mote T. 2007. Trends in snow ablation over North America. *Int. J. Clim. 27*, 739-748, doi:10.1002/joc.1426.

Foster J., Robinson D., Hall D. & Estilow T. 2008. Spring snow melt timing and changes over Arctic lands. *Polar Geogr. 31*, 145-157.

Ge Y. & Gong G. 2008. Observed inconsistencies between snow extent and snow depth variability at regional/continental scales. *J. Clim. 21*, 1066-1082, doi:10.1175/2007JCLI1829.1.

Global Soil Data Task. 2000. Global Soil Data Products CD-ROM (IGBP-DIS), CD-ROM, International Geosphere-Biosphere Programme, Data and Information System, Potsdam, Germany. Available from Oak Ridge National Laboratory Distributed Active Archive Center, Oak Ridge, Tennessee, U.S.A.

Gong G., Entekhabi D., Cohen J. & Robinson D. 2004. Sensitivity of atmospheric response to modeled snow anomaly characteristics. *J. Geophys. Res. 109*, D06107, doi:10.1029/2003JD004160.

Grippa M., Kergoat L., Le Toan T., Mognard N., Delbart N., L'Hermitte J. & Vicente-Serrano S. 2005. The impact of snow depth and snowmelt on the vegetation variability over central Siberia. *Geophys. Res. Lett. 32*, L21412, doi:10.1029/2005GL024286.

Groisman P., Karl, T. & Knight R. 1994. Changes of snow cover, temperature, and radiative heat balance over the Northern Hemisphere. *J. Clim. 7*, 1633-1656.

Groisman P., Knight R., Razuvaev V., Bulygina O. & Karl T. 2006. State of the gound: climatology and changes during the past 69 years over Northern Eurasia for a rarely used measure of snow cover and frozen land. *J. Clim. 19*, 4933-4955.

Hirabayashi Y., Kanae S., Struthers I. & Oki T. 2005. A 100-year (1901-2000) global retrospective estimation of terrestrial water cycle. *J. Geophys. Res. 110*, doi:10.1029/2004JD005492.

Hirabayashi Y., Kanae S., Motoya K., Masuda K. & Doll P. 2008. A 59-year (1948-2006) global near-surface meteorological data set for land surface models. Part I: Development of daily forcing and assessment of precipitation intensity. *Hydrol. Res. Lett. 2*, 36-40.

Howell S., Duguay C. & Markus T. 2009. Sea ice conditions and melt season duration variability within the Canadian Arctic Archipelago: 1979-2008. *Geophys. Res. Lett. 36*, L10502, doil:10.1029/2009GL037681.

Iijima Y., Fedorov A., Park H., Suzuki K., Yabuki H., Maximov T. & Ohata T. 2010. Abrupt increases in soil temperatures following increased precipitation in a permafrost region, central Lena river basin, Russia. *Permafrost and Periglac. Process. 21*, 30-41.

Isard S., Angel J. & VanDyke G. 2000. Zones of origin for Great Lakes cyclones in North America, 1899-1996. *Mon. Weather Rev. 128*, 474-485.

Jordan R. 1991. A one-dimensional temperature model for a snow cover: Technical documentation for SNTHERM.89. U.S. Army Cold Regions Research and Engineering Laboratory, Special Report 91-116.

Kitaev L., Forland E., Razuvaev V., Tveito O. & Krueger O. 2005. Distribution of snow cover over Northern Eurasia. *Nord*. *Hydrol*. *36*, 311-319.

Lindsay R., Zhang J., Schweiger A., Steele M. & Stern H. 2009. Arctic sea ice retreat in 2007 follows thinning trend. *J. Clim*. *22*, 165-176,

Llody a. & Fastie C. 2002. Spatial and temporal variability in the growth and climate response of treeline trees in Alaska. *Clim*. *Change*. *52*, 481-509.

McDonald K., Kimball J., Njoku E., Zimmermann R. & Zhao M. 2004. Variability in springtime thaw in the terrestrial high latitudes: Monitoring a major control on the biospheric assimilation of atmospheric CO2 with spaceborne microwave remote sensing. *Earth Interact*. *8*, 1-20.

Meador W. & Weaver W. 1980. Two-stream approximations to radiative transfer in planetary atmospheres: A unified description of existing methods and a new improvement. *J. Atmos*. *Sci*. *37*, 630-643.

Nelson F, Shiklomanov N., Mueller G., Hinkel K., Walker D. & Bockheim J. 1997. Estimating active-layer thickness over a large region: Kuparuk River basin, Alaska, U.S.A. *Arct. Alp. Res.*, *29*(*4*), 367-378.

Park H, Iijima Y., Yabuki H., Ohta T., Walsh J., Kodama Y., & Ohata T. 2011. The application of a coupled hydrological and biogeochemical model (CHANGE) for modeling of energy, water, and CO2 exchanges over a larch forest in eastern Siberia. *J. Geophys. Res.* 116, D15102, doi:10.1029/2010JD015386.

Pomeroy J., Marsh P. & Gray D. 1997. Application of a distributed blowing snow model to the Arctic. *Hydrol. Processes. 11*, 1451-1464.

Pomeroy J. & Li L. 2000. Prairie and arctic areal snow cover mass balance using a blowing snow model. *J. Geophys. Res. 105*(*D21*), 26,619-26,634.

Ramankutty N. & Foley J. 1999. Estimating historical changes in global land cover: Croplands from 1700 to 1992. *Global Biogeochem. Cycles. 13*(*4*), 997-1027.

Robinson D., Dewey K. & Heim R. 1993. Global snow cover monitoring: An update. *Bull. Am. Meteorol. Soc. 74*, 1689-1696.

Saito K. & Cohen J. 2003. The potential role of snow cover in forcing interannual variability of the major Northern Hemisphere mode. *Geophys. Res. Lett. 30*, 1302, doi:10.1029/2002GL016341.

Saito K., Yasunari T. & Cohen J. 2004. Changes in the sub-decadal co-variability between Northern Hemisphere snow cover and the general circulation of the atmosphere. *Int. J. Clim. 24*, 33-44.

Screen J. & Simmonds I. 2010. The central role of diminishing sea ice in recent Arctic temperature amplification. *Nature. 464*(*29*), doi:10.1038/nature09051.

Serreze M., Bromwich D., Clark M., Etringer A., Zhang T. & Lammers R. 2003. Large-scale hydro-climatology of the terrestrial Arctic drainage system. *J. Geophys. Res.* 108(D2), 8160, doi:10.1029/2001JD000919.

Serreze M. & Francis J. 2006. The polar amplification debate. *Clim. Change. 76*, 241-264.

Stieglitz M., Dery S., Romanovsky V. & Osterkamp T. 2003. The role of snow cover in the warming of Arctic permafrost. *Geophys. Res. Lett.*, *30*(*13*), 1721, doi:10.1029/2003GL017337.

Storck P., Lettenmaier D. & Bolton S. 2002. Measurement of snow interception and canopy effects on snow accumulation and melt in a mountainous maritime climate, Oregon, united states. *Water Resour. Res. 38*, doi:10.1029/2002WR001281, 2002.

Wigmosta M. & Lettenmaier D. 1994. A distributed hydrology-vegetation model for complex terrain. *Water Resour. Res.* 30, 1665-1679.

Yang D., Robinson D., Zhao Y., Estilow T. & Ye B. 2003. Streamflow response to seasonal snow cover extent changes in large Siberian watersheds. *J. Geophys. Res. 108*(D18): 4578, doi:10.1029/2002JD003149.

Ye H. 2001. Increases in snow season length due to earlier first snow and later last snow dates over North Central and Northwest Asia during 1937-94. *Geophys. Res. Lett. 28*(*3*), 551-554.

Figure captions

Figure 1. Schematic of snow processes represented in CHANGE.

Figure 2. Interannual variability of (a) wintertime (October to March) surface air temperature (SAT) and (b) precipitation, each during the period 1948–2006.

Figure 3. Interannual variability of monthly surface air temperature anomalies over the Arctic lands during the period 1948–2006.

Figure 4. (a) Location map of GSOD sites selected for validating the simulated snow depth. (b) Comparison between the observed and simulated snow depths averaged for JFM. In the map (a), the colors indicate correlation coefficients between the observations and simulations at ≥ 95% confidence level. In the plot (b), horizontal and vertical bars represent the standard deviations of observations and simulations for snow depth, respectively.

Figure 5. Distribution of average snow depth for JFM over the period 1948–2006 (a) and the trend derived by a linear analysis (b).

Figure 6. Interdecadal variations in snow depth anomaly. Each anomaly is defined as the difference between the average during 1948–2006 and that during the 10-year

period.

Figure 7. Interannual variability of anomalies in (a) snow accumulation dates in the fall and (b) snow disappearance dates in the spring. The white areas in high latitudes mean the range-over of the maximum.

Figure 8. Variations of (a) averaged monthly snow cover extent derived from both NOAA weekly datasets and the model results and (b) monthly snow depth based on the simulated results.

Figure 9. Interannual variability of snow cover extent over the Arctic lands at the defined snow depth levels. The numbers within the axes represent the average snow cover extent (10^6 km^2) during 1948–2006 as calculated from the simulation results.

Figure 10. Comparison between snow cover extents of 1961–1970 and 2001–2006 at snow depth levels of (a) < 6 cm and (b) ≥ 36 cm. Brown color in the figures means the area that SCE of each SD coexisted during the two periods. Blue and green indicate the extended area of SCE during 1961-1970 and 2001-2006, respectively.

Figure1

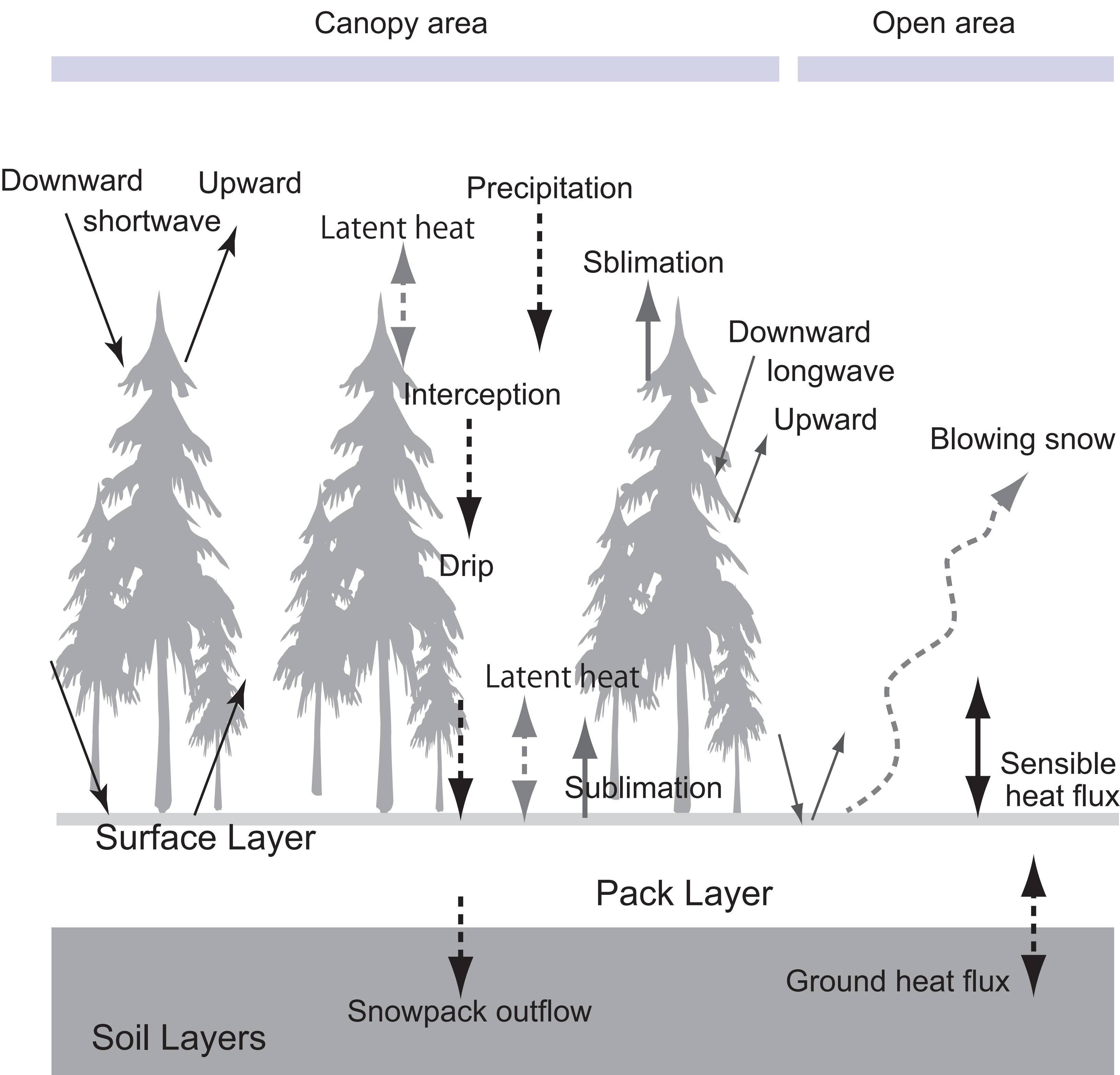

Canopy area
Open area
Downward
shortwave
Upward
Latent heat
Precipitation
Sblimation
Downward
longwave
Upward
Interception
Blowing snow
Drip
Latent heat
Sublimation
Sensible
heat flux
Surface Layer
Pack Layer
Ground heat flux
Snowpack outflow
Soil Layers

Figure2

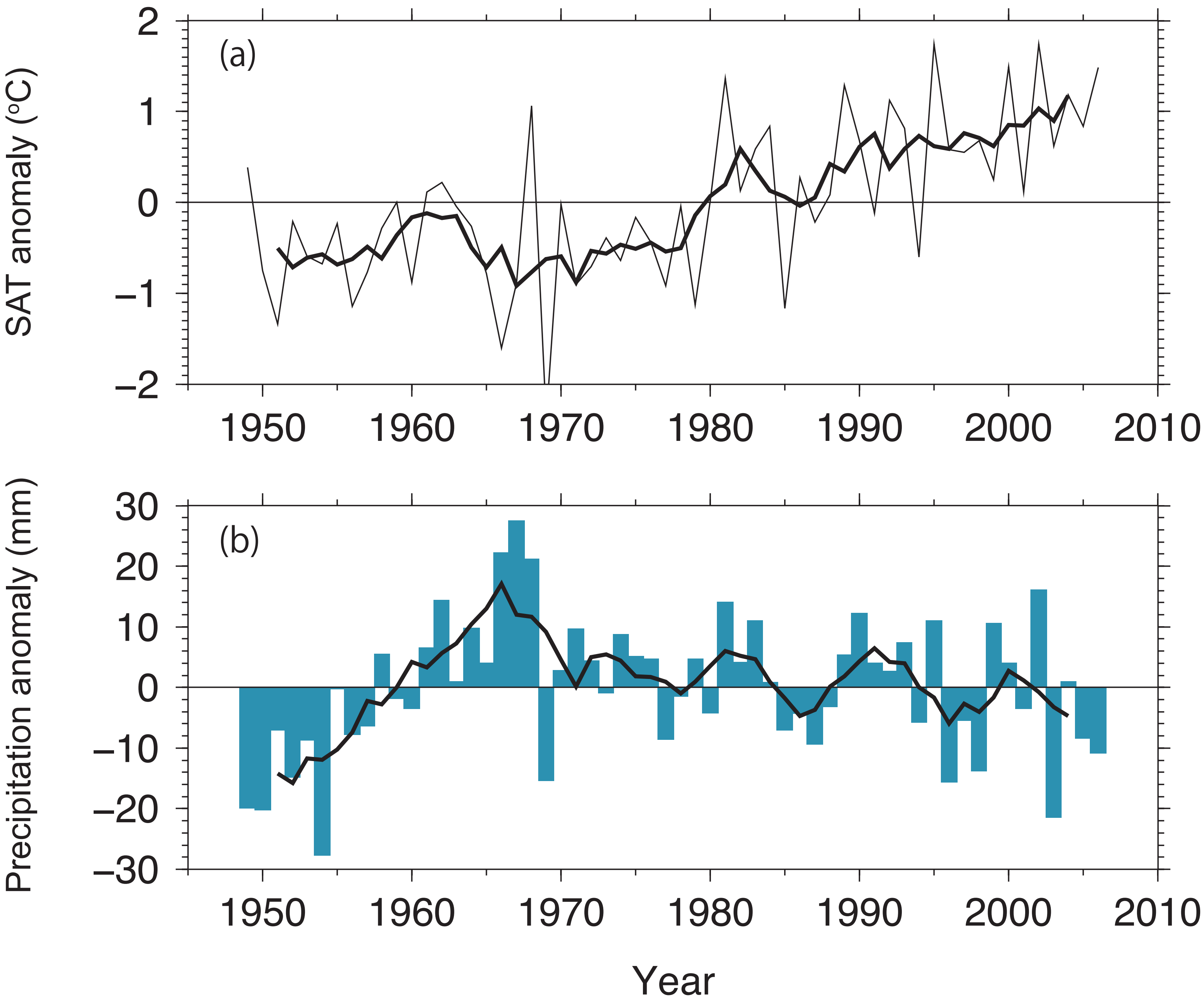

(a)
SAT anomaly (ºC)
2
1
0
−1
−2
1950
1960
1970
1980
1990
2000
2010
(b)
Precipitation anomaly (mm)
30
20
10
0
−10
−20
−30
1950
1960
1970
1980
1990
2000
2010
Year

Figure3

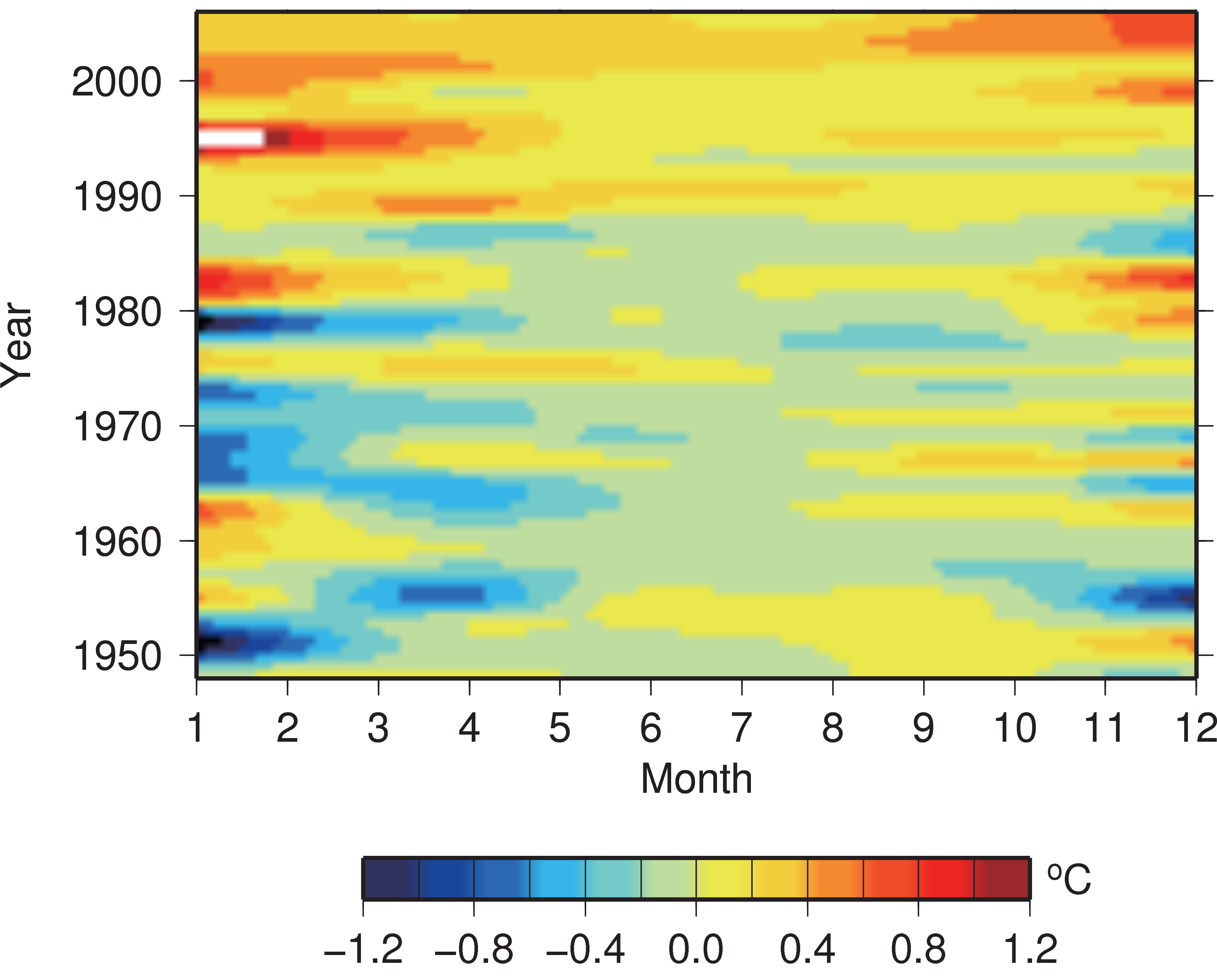

2000
1990
1980
1970
1960
1950
Year
1
2
3
4
5
6
7
8
9
10
11
12
Month
−1.2
−0.8
−0.4
0.0
0.4
0.8
1.2
oC

Figure4

(a)

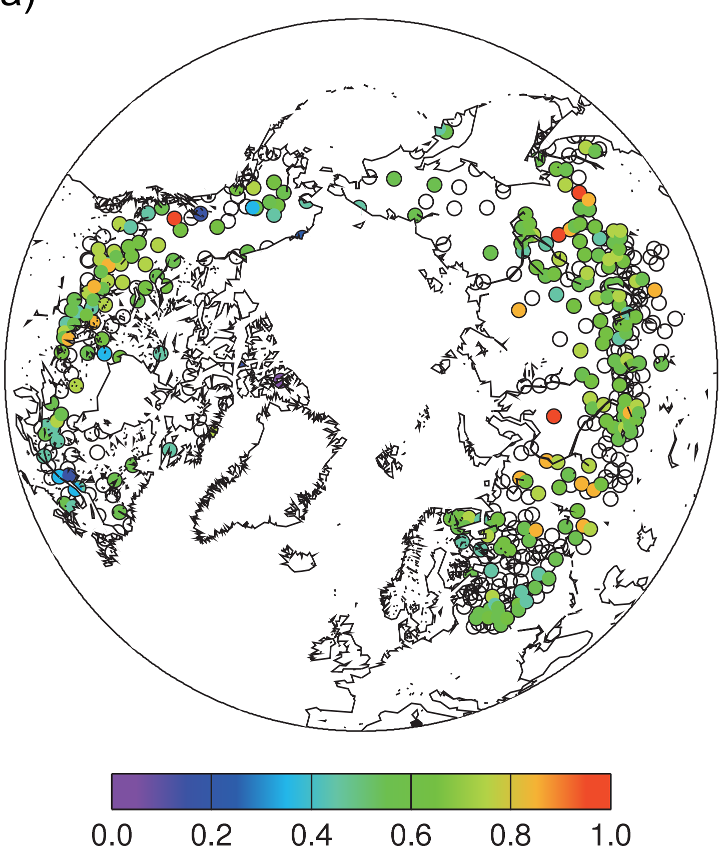

0.0
0.2
0.4
0.6
0.8
1.0

(b)

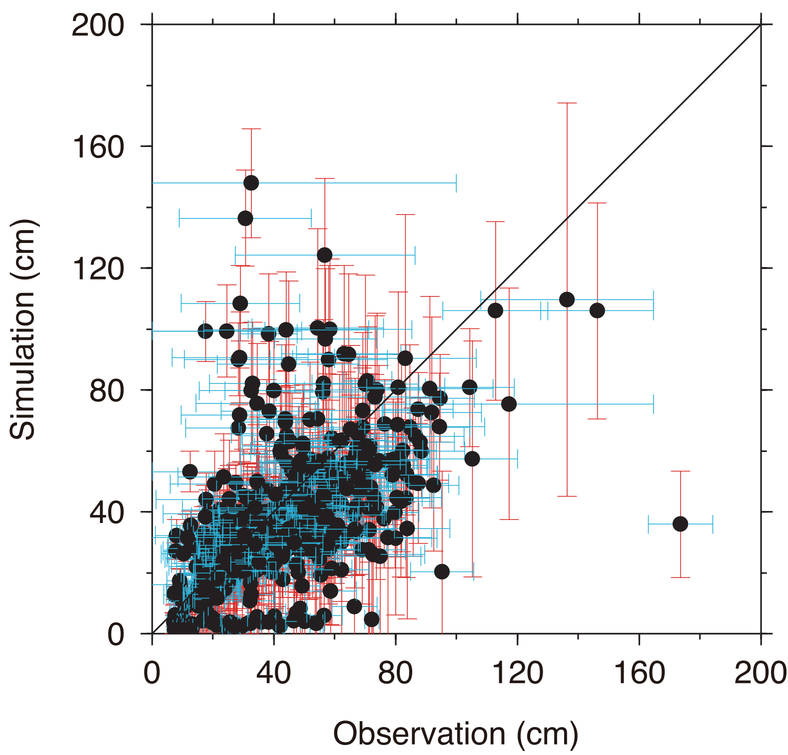

200
160
120
80
40
0
Simulation (cm)
0
40
80
120
160
200
Observation (cm)

Figure5

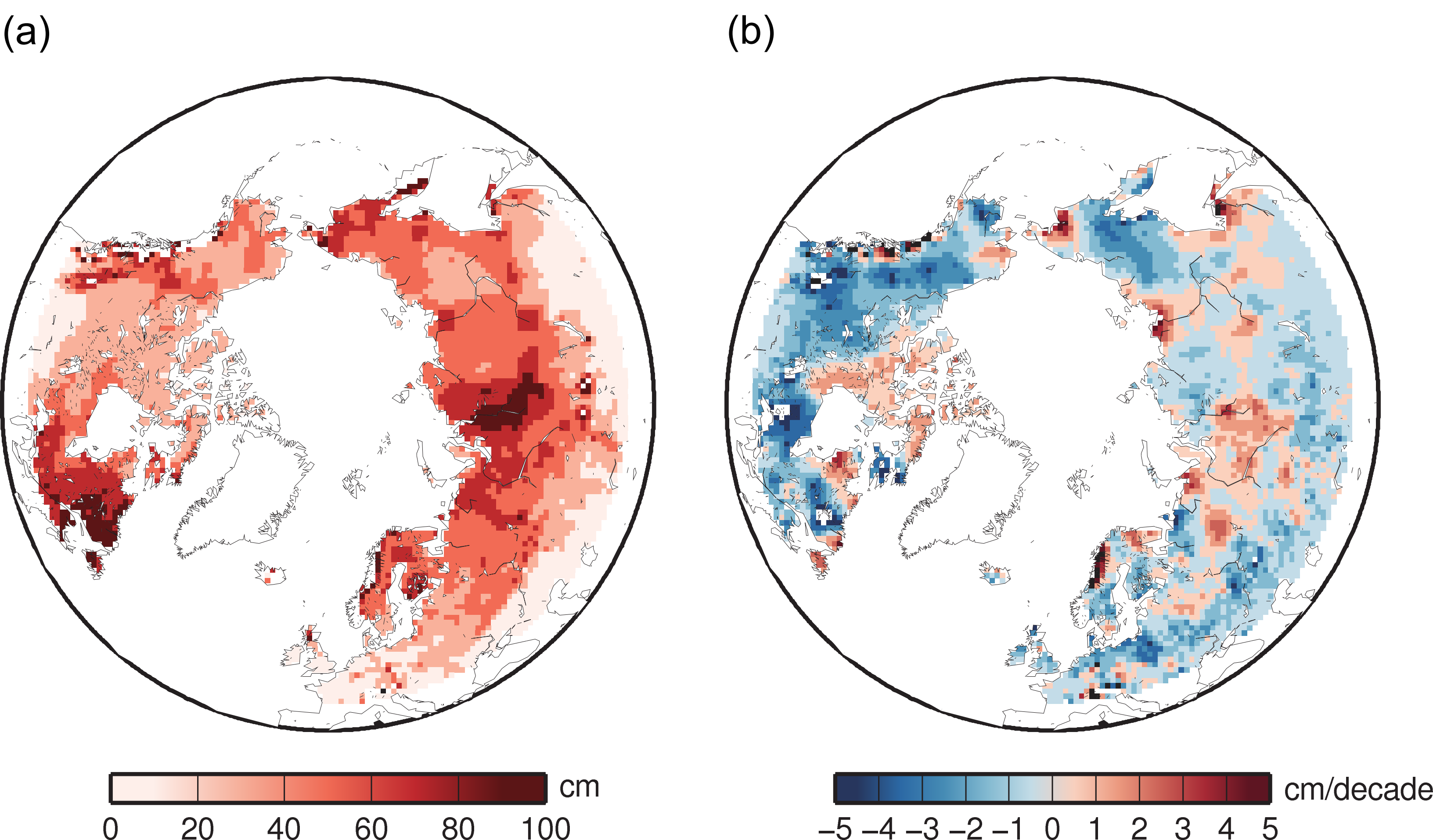

Figure6

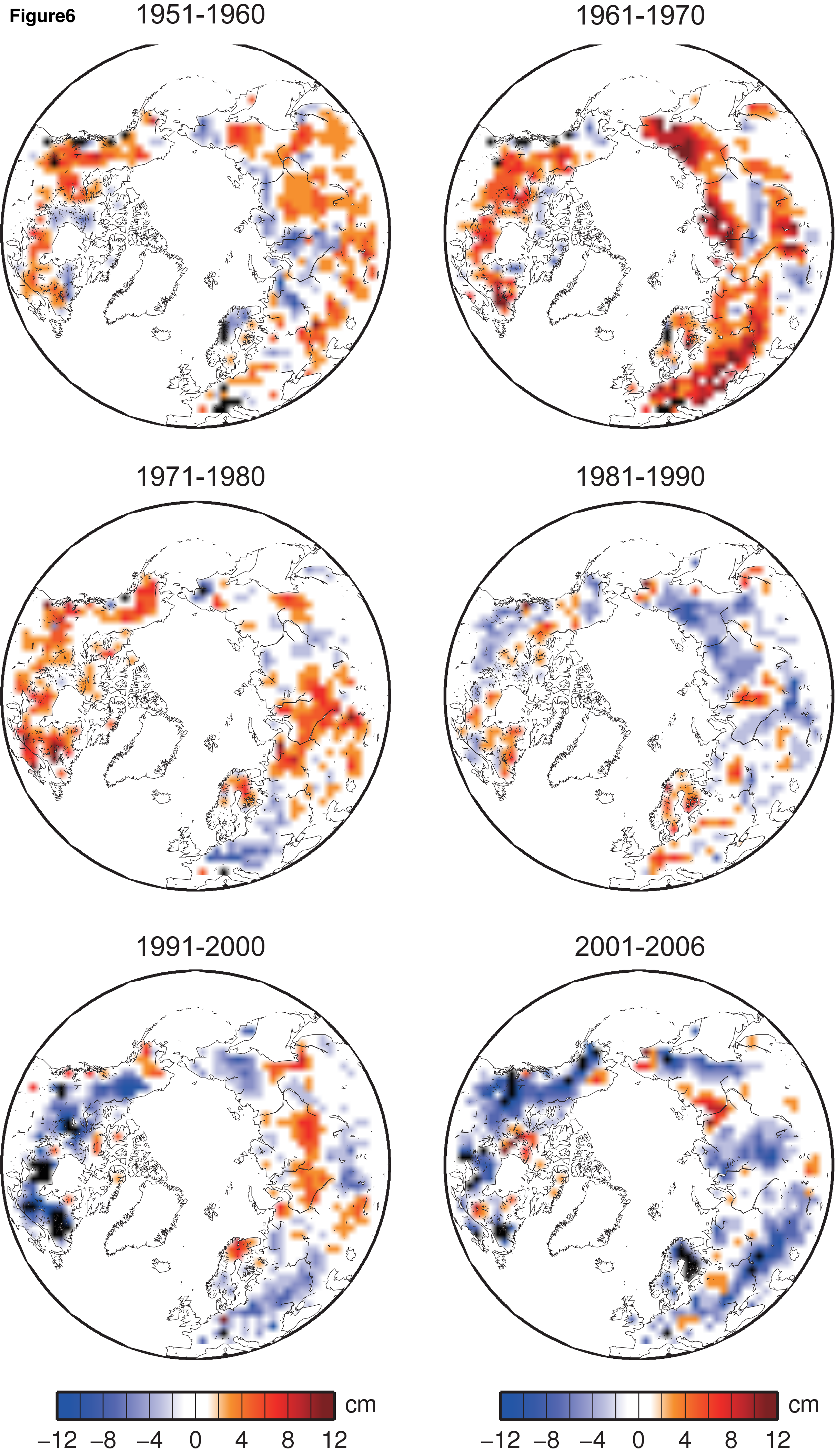
1951-1960
1961-1970
1971-1980
1981-1990
1991-2000
2001-2006
cm
−12 −8 −4 0 4 8 12
cm
−12 −8 −4 0 4 8 12

Figure7

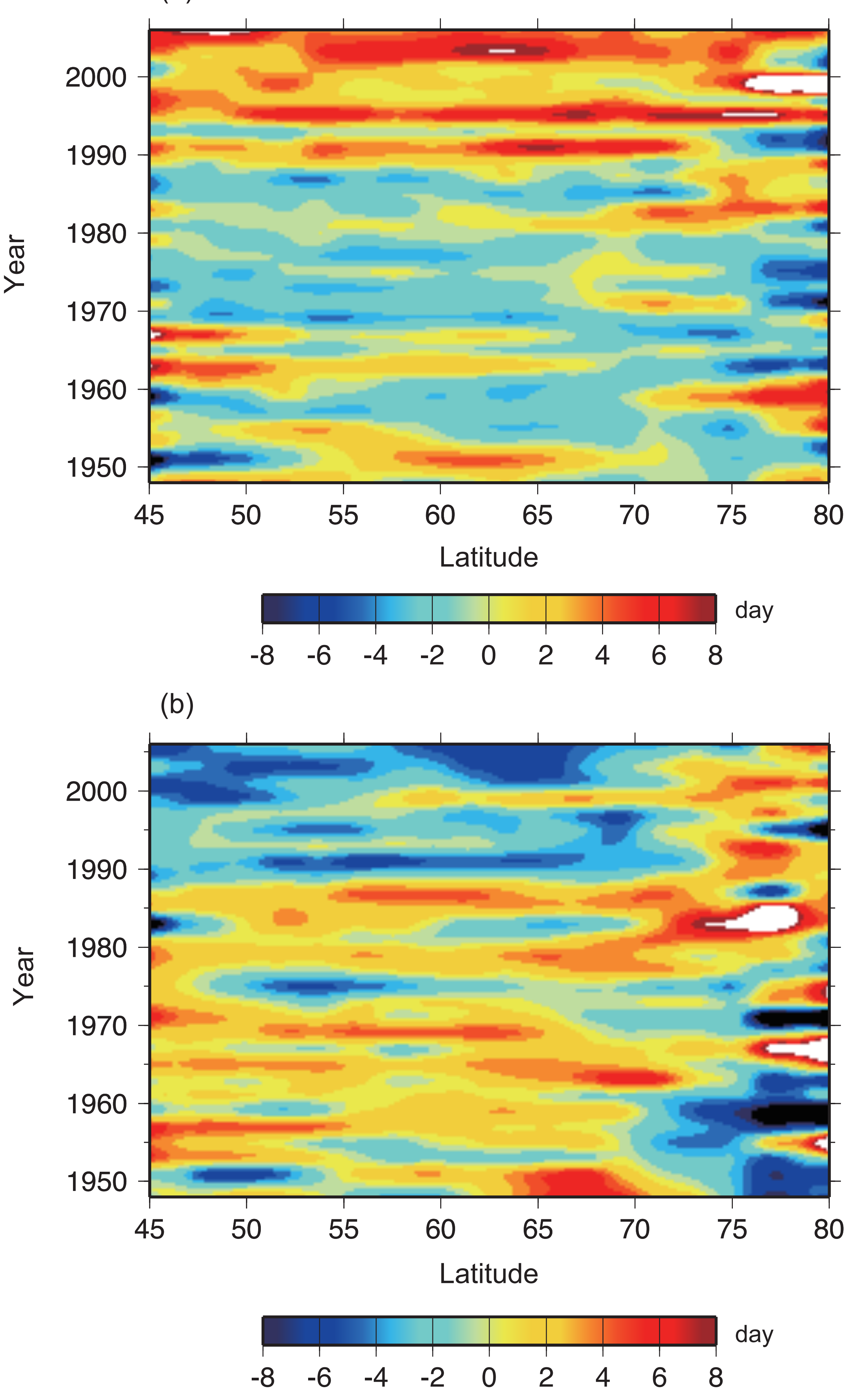

(a)
Year
2000
1990
1980
1970
1960
1950
45
50
55
60
65
70
75
80
Latitude
day
-8
-6
-4
-2
0
2
4
6
8
(b)
Year
2000
1990
1980
1970
1960
1950
45
50
55
60
65
70
75
80
Latitude
day
-8
-6
-4
-2
0
2
4
6
8

Figure8

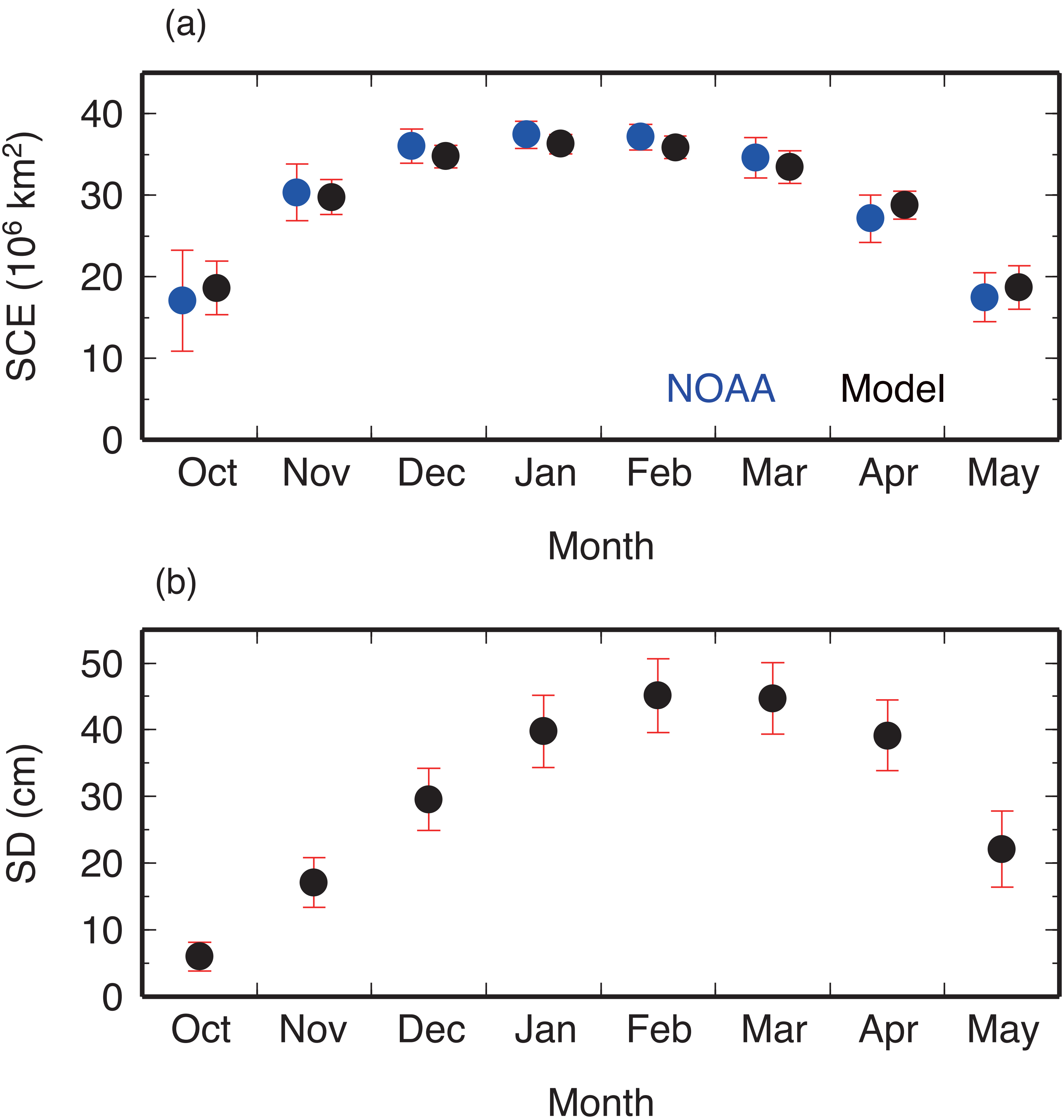
(a)
40
30
20
10
0
SCE (10^6 km^2)
NOAA
Model
Oct
Nov
Dec
Jan
Feb
Mar
Apr
May
Month
(b)
50
40
30
20
10
0
SD (cm)
Oct
Nov
Dec
Jan
Feb
Mar
Apr
May
Month

Figure9

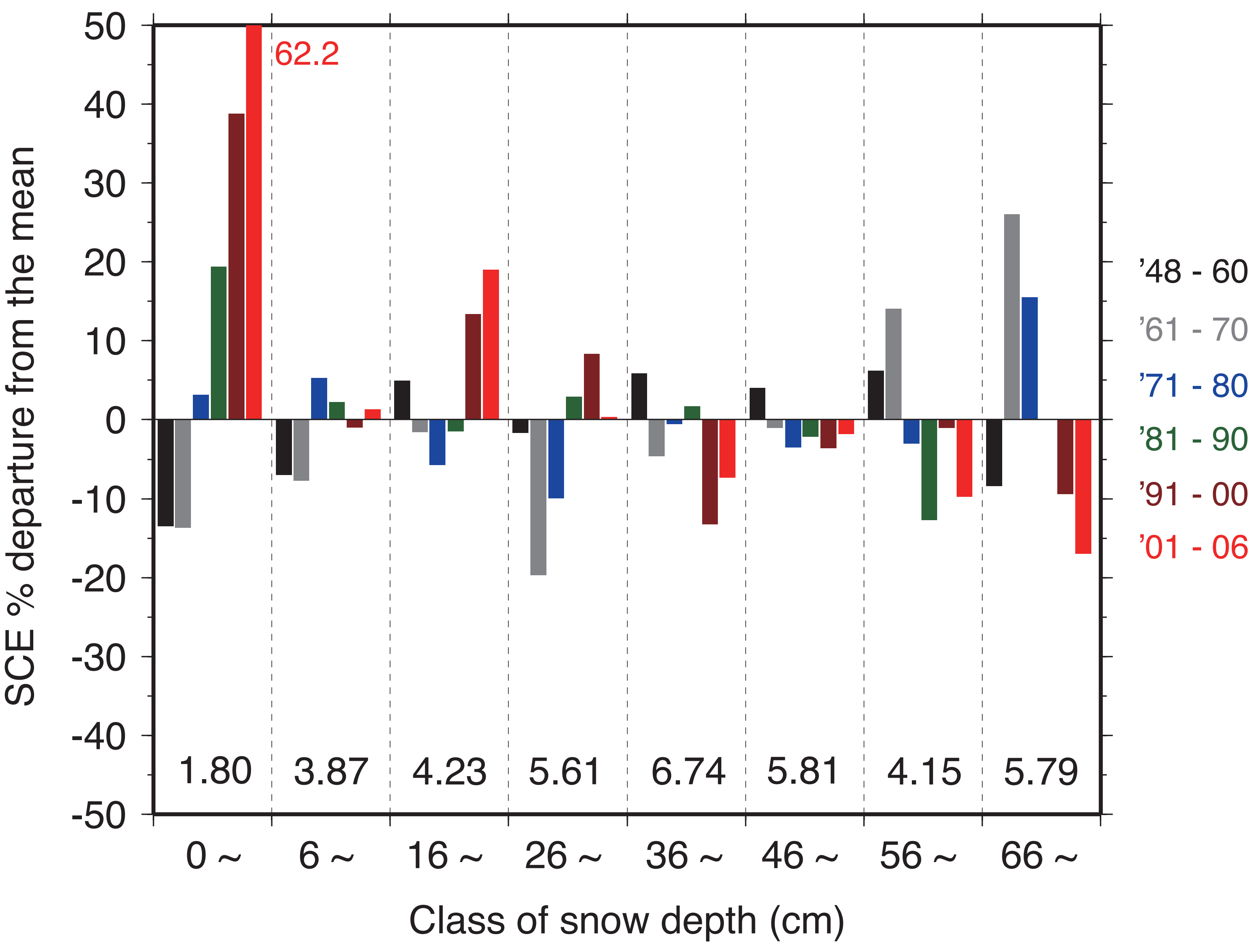

50
40
30
20
10
0
-10
-20
-30
-40
-50
SCE % departure from the mean
62.2
1.80
3.87
4.23
5.61
6.74
5.81
4.15
5.79
0 ~
6 ~
16 ~
26 ~
36 ~
46 ~
56 ~
66 ~
Class of snow depth (cm)
'48 - 60
'61 - 70
'71 - 80
'81 - 90
'91 - 00
'01 - 06

Figure10

(a)

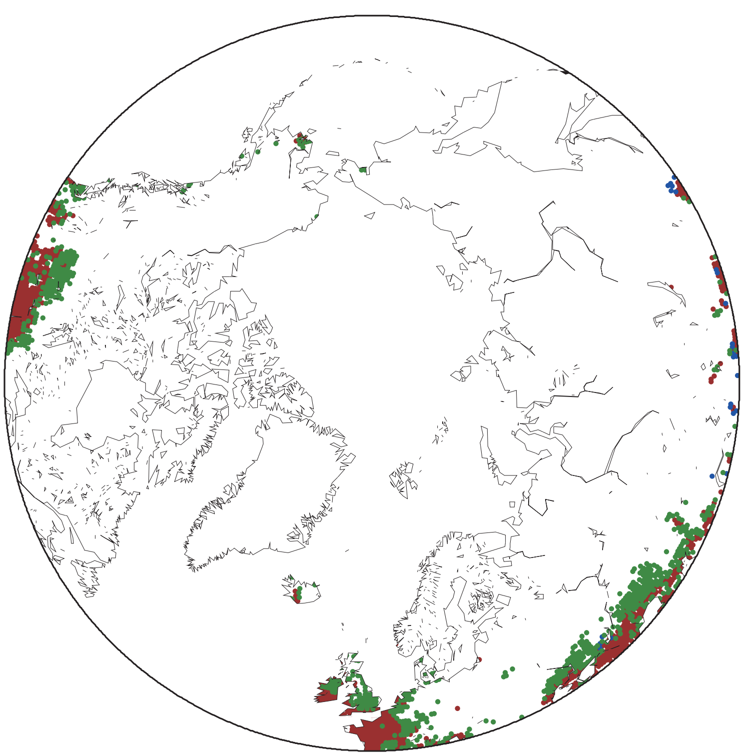

(b)